



**HAL**  
open science

# Dynamics of a 2D vibrated model granular gas in microgravity

Georges Bossis, Y Grasselli, Alain Meunier, O Volkova

► **To cite this version:**

Georges Bossis, Y Grasselli, Alain Meunier, O Volkova. Dynamics of a 2D vibrated model granular gas in microgravity. M.G. Sakellariou. Granular materials, 2017, granular materials. hal-03570935

**HAL Id: hal-03570935**

**<https://hal.science/hal-03570935v1>**

Submitted on 13 Feb 2022

**HAL** is a multi-disciplinary open access archive for the deposit and dissemination of scientific research documents, whether they are published or not. The documents may come from teaching and research institutions in France or abroad, or from public or private research centers.

L'archive ouverte pluridisciplinaire **HAL**, est destinée au dépôt et à la diffusion de documents scientifiques de niveau recherche, publiés ou non, émanant des établissements d'enseignement et de recherche français ou étrangers, des laboratoires publics ou privés.

# 1 Dynamics of a 2D vibrated model granular gas in microgravity

document.Macro

B. Bossis<sup>(1)</sup>, Y. Grasselli<sup>(2)</sup>, A. Meunier<sup>(1)</sup>, O. Volkova<sup>(1)</sup>

<sup>1</sup>Laboratoire de la Matière Condensée, University of Nice Sophia Antipolis, CNRS UMR 7336, Parc Valrose, 06108 Nice cedex 2, France

<sup>2</sup>SKEMA Business School, Université de la Côte d'Azur, 60 rue Dostoievski, CS30085, 06902 Sophia-Antipolis, France

**Abstract:** We present an experimental work performed on a vibrated granular gas enclosed into a 2D-cell. Experimental investigations are performed in microgravity during parabolic flights. High speed video recording and optical tracking allow to obtain the full kinematics of the particles allowing the determination of all inelastic parameters as well as the translational and rotational velocity distributions. The energy input into the medium is performed by submitting the experimental cell to an external and controlled vibration. Two model gas are studies: beads and disks; the latter being used to study the rotational part of the particle's dynamics. We report that the free cooling of a granular medium can be predicted if we consider the velocity dependence of the restitution coefficient and that the experimental ratio of translational versus rotational temperature decreases with the density of the medium but increases with the driving velocity of the cell. These experimental results are compared with existing theories. We also introduce a model which fairly predicts the equilibrium temperatures along the direction of vibration.

**Keywords:** Granular, microgravity; translational temperature, rotational temperature

## 1. Introduction

document.\* document.cceptAllChangesShown

## 2. Free cooling

The cooling of a granular gas can be investigated by considering a granular medium submitted to a continuous external energy input (generally done by submitting the medium to a controlled vibration), then removing it and observing how the medium goes back to rest. Experimental studies on granular have to deal with gravity effects and studying model particles (disks in general) on an air flow table can overcome gravitational effects. Our approach was to perform experiments in a low-gravity environment by boarding the experimental apparatus in the Airbus Zero-G from Novespace. The airplane undergoes successive parabolic flights allowing around 22s of microgravity per parabola. The relative gravity is recorded during the flight (fig. 1) allowing to monitor the quality of microgravity environment.

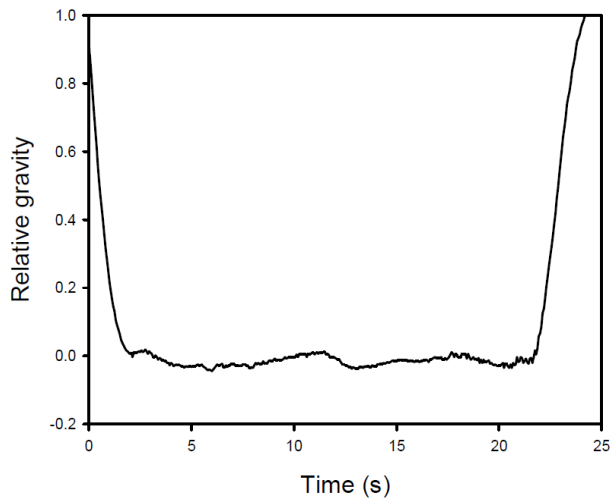


Figure 1. Typical behaviour of the relative gravity during a parabola. These curves are used to check the quality of the microgravity environment.

The medium is composed of iron beads with radius  $a=1$  mm, enclosed in a 2D cell (fig. 2). The initial volume fraction of the medium is  $\beta$  %. The cell was chosen with a rounded shape in order to ensure a homogeneous injection of energy in the system in the presence of the vibration. The cell's walls are made of glass in order to cancel electrostatic effects and to minimize the friction between the beads and the walls. The cell is mounted on a vibrating device ("Modal exciter, 100N, Bruel & Kjaer") to allow periodic (sine oscillations) external vibrations with different frequencies,  $\nu$ , and amplitudes  $A$  to be applied on the medium. The maximum cell's velocities can be changed from 30 cm/s up to 250 cm/s. Note that, this experimental situation permits us to avoid density fluctuations like the ones occurring in fluidized beds or strong rolling contributions as the ones encountered in horizontal studies where the particles move over a horizontal vibrated plate. The 2D configuration also forbids the cross-over of particles trajectories. The motion of granular particles is recorded with the

help of a high-speed camera at 470 frames per seconds during about 6s, giving us a collection of about 3000 pictures per experiment with a picture dimension of 320×320 pixels.

The high speed video recording allows us to track each particle and then to get access to their positions inside de cells. From this knowledge, the dynamics of the medium can be retrieved through the velocities of each particle. The experimental processing is performed by image analysis. Each particle  $p$  is tracked individually allowing to obtain the positions  $x_p(t)$  and  $y_p(t)$  as a function of time. It is interesting to note that from these sets of coordinates all experimental parameters required to describe the collective motion can be directly determined such as the velocities components, the normal restitution coefficient,  $e$ , but also the pair correlation function  $g(r)$  (fig. 3).

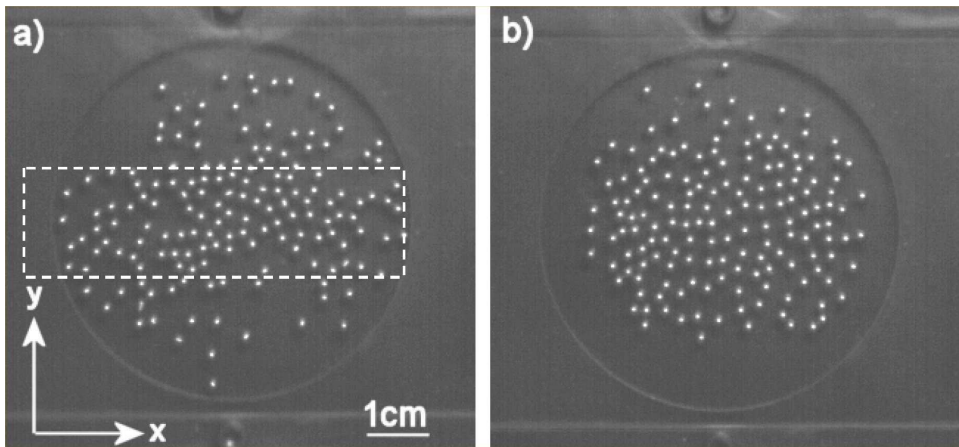


Figure 2. Snapshots of the experimental cell. The external vibration is applied along the y-direction (direction of the normal gravity). High speed video recording is used to track the motion of each individual particle. a) Vibration is on: the central part of cell contains an almost constant density of particles (dashed region). b) The external vibration has been stopped and the overall motion of particles stops due to the inelastic collisions.

The maximum value of  $g(r)$  is achieved at the particle diameter which justify that undesired electrostatic effects may be neglected. Note that the small non-zero value of the pair correlation function “before” the particle diameter comes from the uncertainty in the determination of particle’s position by image processing.

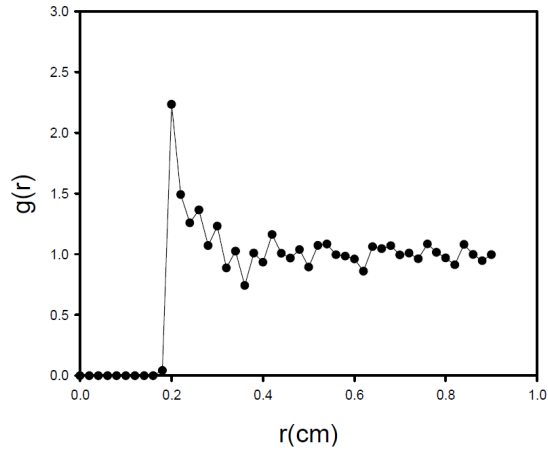


Figure 3. Experimental pair correlation function  $g(r)$  retrieved from the positions of the particles. This curve is averaged over all pictures recorded and on the spatial configurations of particles in the central area of the cell.

In order to study the free cooling, i.e. to relate the loss of energy of the medium due to the inelastic collisions in between particles, the external vibration is switched on prior the microgravity occurs. In zero- $g$ , the particles will then fill the entire region of the cell setting and the video recording is started. After few seconds, the external vibration is switched off and we observe the return to equilibrium (particles at rest throughout the cell). It is worth noting that in the presence of the vibration two types of different regions clearly appear in the cell: two hot (and dilute) regions at the top and bottom of the cell while a dense region exists in the center of the cell (dashed area shown in figure 2a). This experimental configuration gives us the possibility to study a homogeneous bed of particles in contact with two hot regions responsible for the energy input. Once the vibration is removed, the particles almost come to rest due to inelastic collisions inducing energy loss. In such cooling granular systems, a well-known effect is the formation of dense clusters of particles. This phenomenon is not clearly observed in our experiments: when the energy input is cancelled we rather observe some alignments of particles along “wavy lines” but not clear regions of high and low density because the main energy loss during collision occurs along the normal direction between two particles. Another reason may come from the rather low initial volume fraction of the particles. Moreover, in experimental situations, some undesired gravity fluctuations still exists giving rise to a collective motion of all particles in a given direction. But a short time after the vibration has been removed; we generally observe that the particles tend to stop in the center of the cell without evidence for clustering. During the recording, we have verified that the concentration in the central part of cell remains constant and we have based all of other study on the dynamics of this area (fig. 4).

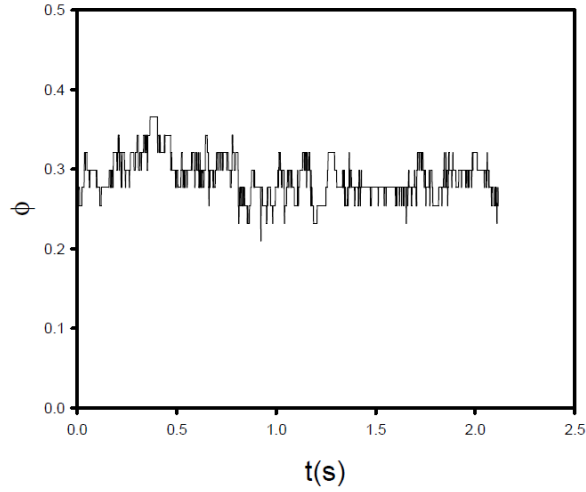


Figure 4. Volume fraction of particles in the central area of the cell as a function of the recording time.

In this region, we will assume that the volume fraction of the granular medium remains constant.

As the behavior of the medium is governed by inelastic collisions, we have determined experimentally the normal restitution coefficient between particles as a function of the relative normal velocities of two colliding particles. We have performed a statistics on two particles collisions (with and without the external vibration) by comparing, on experimental trajectories, the directions and the magnitudes of the velocities before,  $T_{rot}$  and after,  $T_y/T_x$  impact. By tracking these changes in the direction of motion of each particle when a nearest neighbor is present, we are able to precisely determine the binary collisions from the trajectories. We can then get the time  $t_c$  at which a collision arises. For the two particles involved in a collision, we consider the previous and following positions from  $t_c$  (fig. 5). The positions considered must insure that the trajectories before and after collision are linear: the determination of the exact position at collision and the direction of the normal direction at contact is then possible and the restitution coefficient is obtained from .

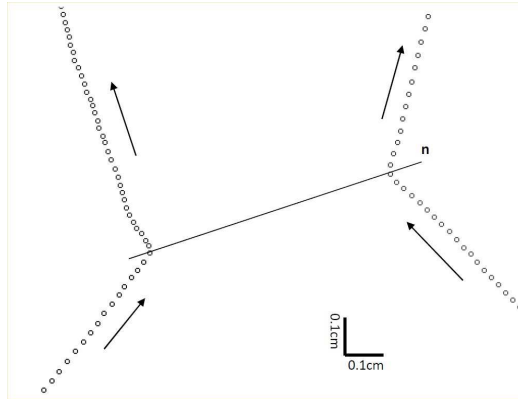


Figure 5. Experimental trajectories recorded during a binary collision between particles. The circles represent the positions retrieved from optical tracking. For a better understanding, we have added on the experimental trajectories the direction of motion of the ~~disk spheres~~ **disk spheres** (arrows) before and after collision. We can precisely obtain the position of each ~~disk sphere~~ **disk sphere** at impact but also the

direction of the normal direction  $\vec{n}$  used in the determination of the inelastic properties.

The behavior of the restitution coefficient vs. the normal relative impact velocity is presented in figure 6. One can note that for high relative velocities we recover the restitution coefficient of 0.9 which is the one usually given for stainless steel beads. The most striking feature is that the restitution coefficient sharply decreases when the impact velocity decreases. This situation is well known in the presence of wet particles where  $e=0$  for Stokes number  $S_i = (m V_i / 6\pi\eta a^2)$  smaller than a critical one,  $S_i \ll S_{i,c}$  [23] and then rises approximately as  $1 - S_{i,c}/S_i$ . This is explained by the viscous dissipation but, for dry particles, most experiments report a decrease of the restitution coefficient when increasing the impact velocity. Actually most of the experiments are made in the presence of gravity with impact velocities larger than 1m/s (for a height  $h=5$  cm the impact velocity of a bead on the plane:  $V_i = \sqrt{2gh}$  is already 1m/s). The restitution coefficient between two dry beads attached by strands in a pendulum device has been investigated [21], the authors also found a lower restitution coefficient at low velocities (typically below 20 cm/s). They interpret this behavior by van der Waals adhesion between the flattened parts of the surface roughness. Our results, obtained in microgravity without experimental drawbacks, well confirm these findings.

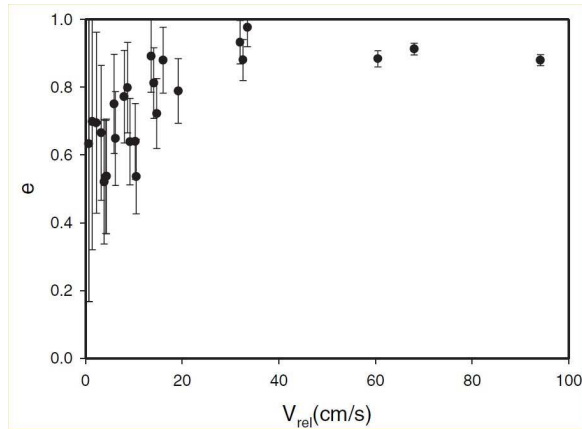


Figure 6. Experimental dependence of the normal restitution coefficient,  $e$ , as a function of the relative normal impact velocity, obtained from the experimental trajectories of the particles. A clear decrease of  $e$  at low impact velocities is observed.

To investigate the free cooling more precisely, a typical record on how the energy decreases once the external energy input has been cancelled is presented in figure 7. This behavior is monitored through the average velocities of the particles in the central area of the cell. One can observe the rapid decay of the average velocity. The non-zero value measured for “long times” comes from the small gravity fluctuations occurring during the parabolic flight.

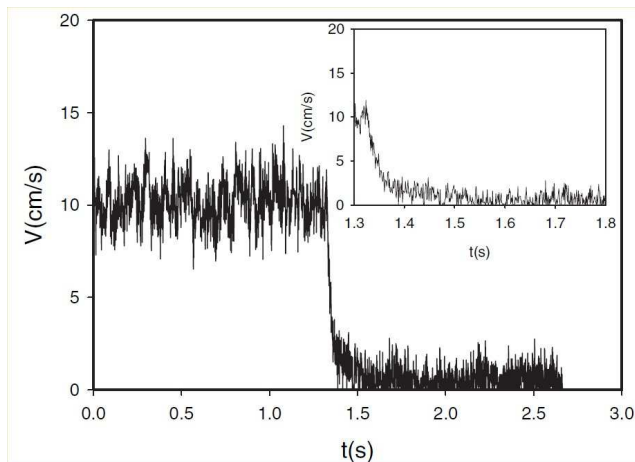


Figure 7. Time dependence of the average translational velocity of the particles calculated from the positions in the central part of the cell. The vibration is cut off during recording and the decay of the energy in the granular system is clearly observed (max cell velocity of 74.6 cm/s). The insert represents a zoom of the curve when the external vibration is stopped.



We can first consider the energy decay assuming a constant restitution coefficient (typically  $e=0.9$  for stainless steel beads). The time dependence of the energy is predicted to behave as

$$E(\tau) = 1/(1+\tau)^2, \quad \tau = (1-e^2)t/t_E \quad \text{where } t_E \text{ is the Enskog time:}$$

$$t_E = (a\sqrt{\pi})/(\sqrt{2}\phi V_0 g(r)). \quad V_0 \text{ is the initial average velocity in the medium.}$$

With our experimental set-up, we can determine experimentally all the parameters involved. A quantitative comparison with experiments is presented in figure 8 (squared symbols) for a cell velocity of 75 cm/s and with the following experimental values:

$$\phi = 0.297 \pm 0.027, \quad V_0 = (0.11 \pm 0.01) \text{ m/s} \quad \text{and} \quad g(r) = 2.23 \pm 0.02$$

$g(r=2a)$ . We see that the decrease of energy observed experimentally is much faster than the one predicted with a constant restitution coefficient. The first possible reason for these differences could come from the friction of the particles on the glass walls of the cell (i.e. an additional loss of energy not due to the inelastic collisions). Nevertheless, a precise analysis of the trajectory of single particles after the vibration has been cut off shows a linear motion at constant speed between two collisions of particles; we may then reject this possibility. The Enskog collision time is  $t_E = 0.0172\text{s}$ . In order to check this value, we have performed a large statistics on our experiments to obtain the average time interval separating two consecutive collisions in the central part of the cell. We found an average time interval of  $(0.0127 \pm 0.0021)\text{s}$  by direct measurements in rather good agreement with the theoretical value.

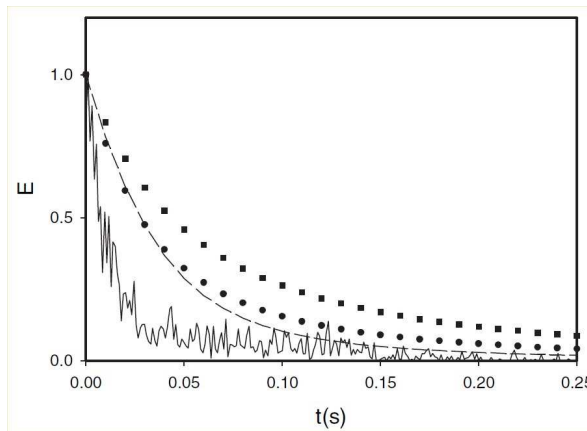


Figure 8. Comparisons between experiments (plain curve) and theory on the energy decay in the granular medium. Black squares: theoretical predictions on the basis of a constant restitution coefficient. Black circles: theoretical predictions including the rotational kinetic energy of the particles. Dashed line: theory considering only the translational part of the energy but including a velocity-dependent restitution coefficient with a similar behavior to the one presented in figure 6.

So, the possible discrepancy between energy decays observed experimentally and the predicted one by theory may come from the presence of the rotational kinetic energy which also dissipates a part of the energy through the surface roughness of the particles [\$\$\$9]. A

tangential restitution coefficient,  $\beta$ , is then introduced to characterize the effect of the rotation of the particles during a collision. In this case, the time dependence of the energy (translational and rotational) is determined from a system of coupled differential equations (eq. (15) in ref. [9]) where all parameters can be obtained experimentally, except  $\beta$ . We have solved numerically this system of equations introducing our experimental results and setting  $\beta=0.1$  (fig. 8, black circles). Note that if we cancel the rotation (i.e.  $\beta=1$ ), the solution is exactly the same as the one predicted with a constant normal restitution coefficient. We can notice that the energy decreases more rapidly but the consideration of the rotational kinetic energy has limited impact –we have checked that it remains small whatever the value of  $\beta$ – and it is still not sufficient to fit the experimental behavior.

To try improving the agreement between theory and experiments, we may consider the velocity dependence of the restitution coefficient. We can express the rate of decrease of the translational kinetic energy  $T$  as  $dT/dt = -n_c(1-e^2)T$  with  $n_c$  the collision rate of binary collisions. In 2D,  $n_c = (2V\phi g(r))/(\pi a)$  with  $V$  the average velocity. Moreover, introducing the normalized energy  $E = T/T_0$  and the velocity ratio  $V/V_0 = T/T_0$ , the rate of decrease of energy can be rewritten in the form:

$$\frac{dE}{dt} = \frac{-g(r)\phi V_0}{a} \sqrt{\frac{2}{\pi}} (1-e(E)^2) E^{3/2} \quad (1)$$

where now  $e$  is assumed to depend on the normal relative velocity. We shall assume that the average relative velocity has the same order of magnitude as the average velocity; then from the curve in figure 6, a fit of the restitution coefficient vs. the normalized energy gives  $e(E) = 0.82 - 0.5 e^{-2.5E}$ . Introducing this last relation in equation (1) and solving it numerically gives the behavior presented in figure 8 (dashed line). Compared to the case including the rotation, we observe a more pronounced decrease of the energy with time. This is understandable since we observed that during cooling the restitution coefficient decreases, increasing the loss of energy. Of course equation (1) is obtained from a crude approximation based on average velocity instead of the probability distribution of velocities, furthermore it is also likely that the tangential restitution coefficient will probably also depend on the relative angular velocities of the colliding particles. A complete theory should include both rotational and translational degrees of freedom with the correct velocity dependence of restitution coefficients.

This first approach on the dynamics of a granular medium shows interesting results but as stated before, the analysis is not complete due to the lack of consideration on rotational effects. With beads and our experimental setup, accessing this data is not possible. We will then introduce in the next part recent experimental investigations based on the same principle but replacing beads by disks in order to obtain a complete description of the dynamical behavior.

### 3. Translational and rotational temperatures

In this part, our aim is to provide experimental data both for the normal and tangential restitution coefficients and for the different quantities related to the rotational and translational degrees of freedom such as the distribution functions and the rotational and translational temperatures. As introduced previously, the kinematics of granular particles submitted to a vertical vibration will still be used in a low gravity environment. We shall particularly focus on the ratio between rotational and translational temperatures. Several other groups have already presented experimental results on granular flow under such conditions [17–20] but to our knowledge this is the first experimental study giving access to rotational and translational velocities and so the corresponding temperatures.

We have designed a 2D-cell of rectangular shape made in Duralumin, with a height  $L_y=6.8\text{cm}$  and a width  $L_x=6\text{cm}$ , wherein brass disks having a diameter  $\sigma=6\text{mm}$  (radius  $a=3\text{mm}$ ) and mass  $m=4.6\cdot 10^{-4}\text{kg}$  are enclosed between two glass plates. The initial area fraction  $\phi$  of the medium is given by the number of disks  $N$  in the cell, here 12 or 24 disks, corresponding, respectively, to area fractions of 8.3% and 16.6%. For this experimental study, we chose this rectangular shape in order to easily monitor the energy input into the medium. The external vibration is still periodic (sine oscillations) with different frequencies,  $\nu$ , and amplitudes  $A$  and it is still applied along the  $y$ -direction (which is the direction of normal gravity). In order to increase the precisions of experimental data, the video recording is performed during the whole parabola and with a higher frame rate (i.e. 900FPS) and higher image resolution (720x720. Pixels); each record gives access to around 22000 pictures per parabola. To reduce friction effects between the disks and the glass plates of the cell, each disk is dressed, on each of its side, by three small steel beads: this configuration also reduces the tilting of the disks in the presence of the external vibration between the cell's plates. The combined thickness of the disks and beads is 3.2mm, for a cell's thickness 3.4mm. The aim of this study is to obtain, by direct optical tracking, the kinematics of the granular particles and thus to access all parameters involved in the dynamics of the medium. The key question being the rotational aspects, each disk is pierced with two small holes, symmetric about the center of the disk and video observations are realized by light transmission (fig. 9).

This setup grants us with images having a high contrast and quality. To determine the position of the disk, we track the trajectories of the two holes of each disk as a function of time. The barycentre then gives the  $x$ - and  $y$ -position of the disk, from which the linear components of the velocity  $v_x(t)$  and  $v_y(t)$  can be computed. The determination of the time dependence of the angle  $\theta(t)$  (fig. 10), computed through the angular position of the holes from the horizontal direction, gives access to the angular velocity  $\dot{\theta}(t)$ .

Since the two holes are well identified during tracking, the orientation angles of the disks are fully determined from 0 to 360 degrees. One can observe in figure 11 a typical experimental record of  $\theta(t)$ . It is interesting to note that a sharp change in the direction of

rotation or a significant variation of the slope, both result from a collision with another particle. On the contrary, when the particle experiences no collision (e.g. time larger than 5 s in fig. 11), the angular velocity remains quite constant, indicating the absence of friction with the lateral walls. During a parabolic flight, the aircraft is subjected to g-jitter along the three directions.

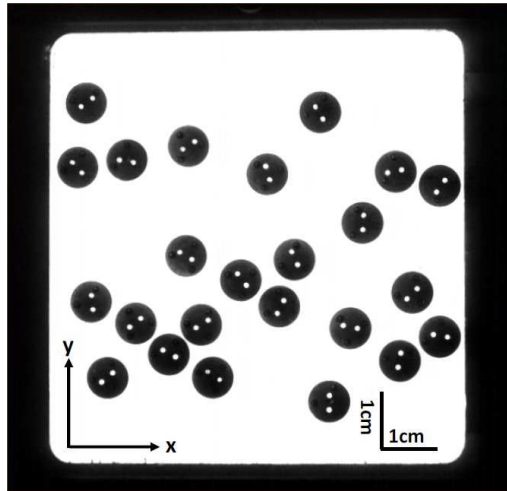


Figure 9. Typical experimental picture recorded during the period of microgravity in the presence of the external vibration (along the y-direction). The two holes, used for the optical tracking of the particles, can be clearly identified. A side and top sketch of one disk is also shown. Three small steel beads are placed on both sides of each disk to reduce friction effect on the lateral walls of the cell and to prevent disk's tilting during vibration.

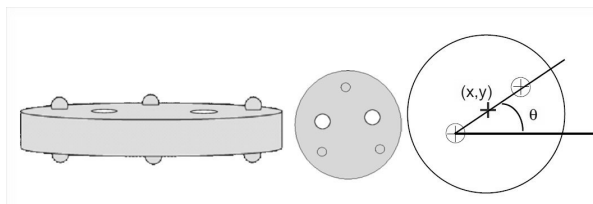


Figure 10. Sketch of the disks used as the model granular particles. Two holes allow optical quality by light transmission. Each disk includes, on both side, six small steel beads to reduce tilting and friction between the vertical walls of the experimental cell. By an optical tracking of the two holes of a disk, the position and orientation angle of the disk can be determined.

~~These fluctuations act on the aircraft and on the devices attached to it but they have no direct action on free floating bodies (like our particles in motion inside the cell). All experimental results presented in this paper were submitted to g-jitter with period of fluctuations of about 1 s and typical amplitudes of 0.01g (cf fig.1). Although these fluctuations may play a role during the collision of the particles with the moving walls of the cell they have limited impact on the motion of particles located "far" from the top and~~

bottom walls and the experimental data used here are retrieved in this area of the cell. The analysis of the trajectory of each disk allows a systematic investigation of inelastic properties of the particles: normal  $e$ , and tangential  $\beta$ , restitution coefficient.

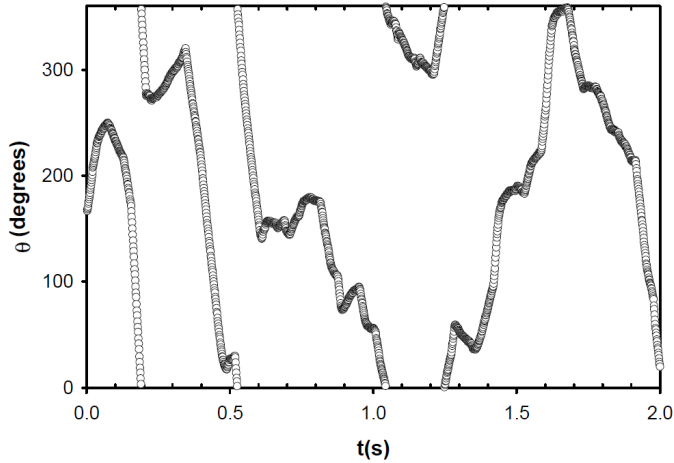


Figure 11. Experimental recording of the angle of orientation,  $\theta$ , of one disk as a function of time in the presence of microgravity and external vibration. A change in the direction of rotation or slope indicates a collision with another particle. When no collision is encountered, the angular velocity remains almost constant.

The collision between disks is processed as we did for the beads in the previous part except that now, the relative velocity includes the rotational part

$$\vec{V}_R = \vec{v}_1 - \vec{v}_2 - a(\vec{\dot{\theta}}_1 + \vec{\dot{\theta}}_2) \times \vec{n}$$

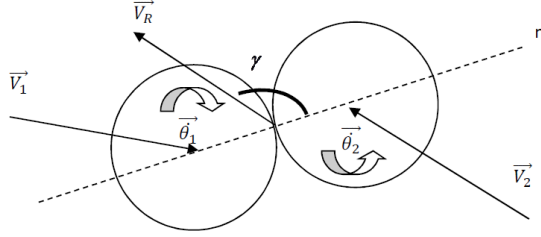
where the subscripts 1 and 2 stand for the two colliding particles at a given time. Again, the normal restitution coefficient is obtained through

$$e = -\frac{|\vec{n} \cdot \vec{V}'_R|}{|\vec{n} \cdot \vec{V}_R|}$$

and the tangential restitution coefficient by

$$\beta = -\frac{|\vec{n} \times \vec{V}'_R|}{|\vec{n} \times \vec{V}_R|}$$

. Another way to express the tangential restitution coefficient is to introduce the angle  $\gamma$  between  $\vec{n}$  and  $\vec{V}_R$  (fig.12), we have for disks the relation [12]:  $1 + \beta = -3(1 + e)\mu \cot(\gamma)$ . The initial slope of  $\beta$  versus  $\cot(\gamma)$  allows the computation of  $\mu$ , the friction coefficient.



We obtained experimentally an average value of  $e = 0.64 \pm 0.03$ .  $r = 0.64 \pm 0.03$  Despite it is sometimes noticed in such situation [22, 23], we did not observe in our experiments any clear dependence of  $e$  on the relative impact velocity. The experimental determination of the restitution coefficient  $\alpha$ , between a particle and the walls of the cell report a value  $\alpha = 0.71 \pm 0.04$ . We were also able to determine the behavior of the experimental tangential restitution coefficient as a function of  $\cot(\gamma)$ . The results are presented in figure 13. From the initial slope one can compute an average value for the friction coefficient during a binary collision:  $\mu = 0.14 \pm 0.01$ . Due to the rectangular shape of the cell and our experimental conditions, most of the binary collisions are head-on collisions so the average value of the tangential restitution can be taken as  $\beta = 0.7 \pm 0.05$ .

Figure 12. Sketch of two colliding particles.  $\vec{v}_1$ ,  $\vec{V}_1$  and  $\vec{v}_2$ ,  $\vec{V}_2$  and,  $\vec{\theta}_1$ ,  $\vec{\theta}_1$  and  $\vec{\theta}_2$ ,  $\vec{\theta}_2$  represent, respectively the linear and rotational velocities of the particles before and after impact.  $\vec{V}_R$  is the relative velocity and  $n$  the normal direction at collision. The impact angle  $\gamma$  is defined from  $n$  to  $\vec{V}_R$ .

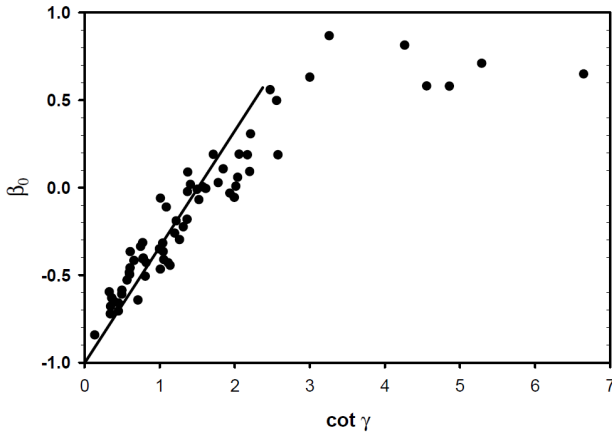


Figure 13. Experimental tangential restitution coefficient  $\beta_0$  as a function of  $\cot(\gamma)$ . This coefficient is calculated from binary collisions with, in addition, the knowledge of the angular velocities of the two disks before and after collision. The plain curve is a linear regression used to compute the friction coefficient arising between two particles at contact.

The density and local velocity profiles of particles within the cell can be determined again from the positions of particles. The local area fraction along the direction of vibration as well as the corresponding velocity profile are reported in figure 14. It is clearly observed that the regions close to the top and bottom walls of the cell show a low concentration of particles while in the center, the area fraction of particles is almost two times the initial one. This result is a direct consequence of inelastic collisions which tend to form clusters of particles [24,25]. As proposed by R. Soto [26], the cell may again be divided into two different parts: one at the center of the cell that we will refer to as “cold” and two ones close to the top and bottom walls, referred to as “hot”, where energy is injected into the medium. In the following, subscripts H and C will be used, respectively, to relate to the “hot” and “cold” regions of the cell. Considering all experiments, we have noticed first, that the values found to characterize the “hot” zone by the height  $h_H$  were not really sensitive to the amplitude of vibration as one could expect, and second that an average value of  $h_H = 9\text{mm} \approx 3.5a$  was acceptable for all the experiments performed. Moreover, computation of the mean free path of particles in the “cold” zone gives a distance of about  $12a$  and  $6a$  (respectively one half and one quarter of the height of the cell) for experiments performed on media containing 12 and 24 particles. These results are achieved by considering the area density in the “cold” zone where typical average values are found of 13% and 30%, respectively, for experiments with 12 and 24 particles. One can then conclude that the collective behavior of particles in the “cold” zone is mainly governed by particle-particle collisions and actually we do not see particles going from one wall to the other without any collision in the bulk. Finally, we have considered the time evolution of density profiles during experimental tracking and it did not show explicitly low-frequency oscillations reported in [27].

The temperature of the granular medium can be computed from the velocities of particles, including the translational  $T_{tr} = mV^2/2$ , and the rotational temperatures

$$T_{rot} = I\omega^2/2 \quad (I \text{ being the moment of inertia of the particles})$$

In a steady state, the temperature of the medium is given by the balance between the energy flux injected into the medium through the collisions of particles with the top and bottom walls of the cell (i.e. in the “hot” regions) and the energy flux dissipated in the bulk (i.e. the “cold” region) due to inelastic collision between particles. Energy injection is then performed in the top and bottom areas of the cell while the main energy dissipation occurs in the central area. Note that all experimental temperatures and data obtained in the following have been measured in the “cold” zone. To obtain reliable measurements, the whole series of images recorded during a parabola (i.e. around 20000 images) are processed for each experimental data given in this paper. We also have to take into account the possible bias due to the presence of jitter during the parabola and we will focus on it during the comparison with theories.

Moreover, from the density profiles, it is possible to determine an average number  $N_H$  of particles present in the “hot” regions of the cell at any time. Finally, the velocity distributions are also obtained from the kinematics of particles. Both typical distributions for translation and rotation velocities are presented respectively on figures 14 and 15. A clear Gaussian behavior is observed. The dashed line on the figures represent the plots of the theoretical expression of the Gaussian distribution in which the experimental values of the squared velocities have been introduced.

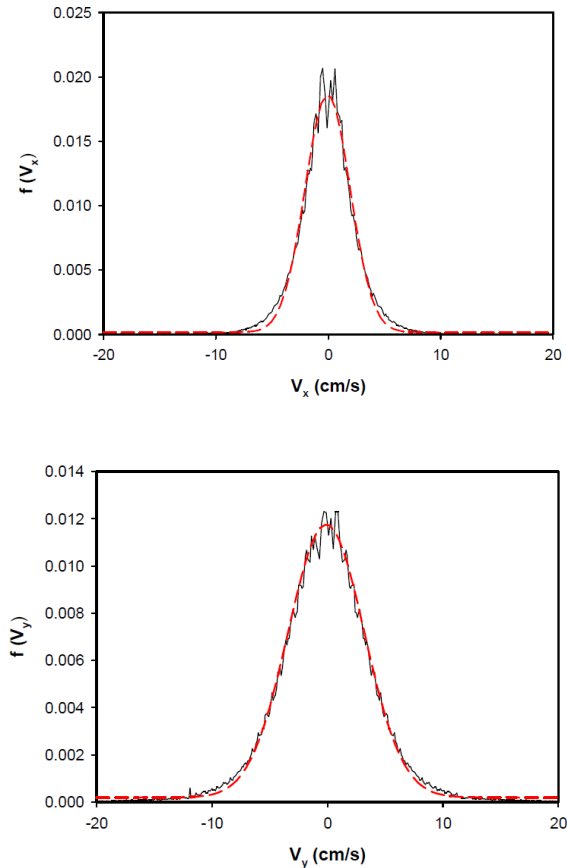


Figure 14. Velocity distributions of the component along the direction of vibration (y-direction) and transverse to it (x- direction). The experimental curves are drawn with plain lines. The dashed lines corresponds to a Gaussian plot of with the average velocity determined experimentally.



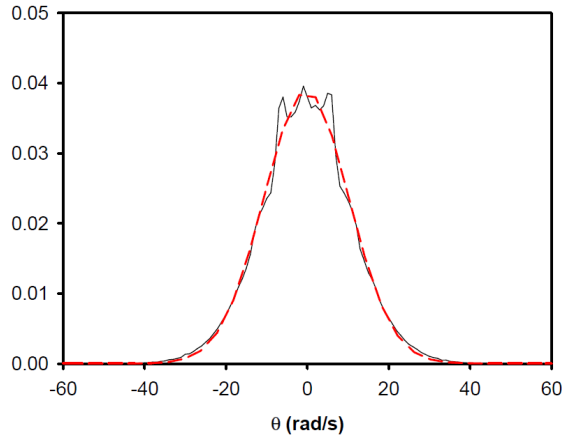


Figure 15. Typical angular velocity distribution of the particles (experiment: plain curve). The dashed line corresponds to the mathematical plotting of a Maxwell distribution which includes the average angular velocity determined experimentally

Due to the rectangular shape of the experimental cell used, and to the relatively low area fraction, the main contribution to the temperature was expected to be found along the direction of the external vibration (the  $y$  – direction). In the following chart we present a summary of the temperature ratios  $T_y/T_x$  and  $T_{tr}/T_{rot}$  with

$T_{tr} = (T_x + T_y)/2$ ,  $T_y/T_x$  in terms of the maximum cell's velocity  $A\omega$   
 $V_{dr} = A\omega$  ( $\omega = 2\pi n$ ) for the two area fractions used. One may note that the ratio  $T_{tr}/T_{rot}$  is not drastically affected if one considers only  $T_y$  as the only contribution to the energy. For the fraction area of 16.6% the ratio  $T_{tr}/T_{rot}$  is ranging from about 4 to 10 for respectively maximum cell velocity from 20cm/s to 40cm/s while  $T_y/T_x$  goes from 2 to 4 maximum. While for the lower fraction area (8.3%),  $T_{tr}/T_{rot}$  is ranging from 11 up to 24 and  $T_y/T_x$  from 5 to 7 only under the same conditions of maximum velocities. We shall analyze these experimental results by focusing first on the ratio  $T_y/T_x$  which is clearly dependent on the area fraction of the medium and is larger for the smallest area fraction. The temperatures found along the direction of vibration are always larger than the ones in the transverse direction which is not a surprising result since the main part of energy injection is performed along the  $y$  – direction and the relatively low area fraction does not allow to redistribute this energy on the perpendicular direction. At low area fraction, the particles can move easily and the  $y$  – direction drives the general motion. On the other hand, we also observe a net increase of the ratio  $T_y/T_x$  with the driving velocity of the cell, but less pronounced for the lower area fraction. However, the driving velocity is not the only parameter of the problem and the amplitude can also play a role. For example, the ratio  $T_y/T_x = 1.98$

reported was achieved with the smallest amplitude ( $A=0.556$  mm) and the largest frequency (60 Hz). For these experimental conditions (large frequency and small amplitude), we observe that the particles mainly concentrate in the center of the cell and consequently the energy injection through the moving walls of the cell is weak. This might explain the low ratio obtained in this experimental run, compared to the one with almost the same value of  $A\omega=0.22$  m/s but a much larger amplitude:  $A=2.3$  mm. For all the other results, the frequency is in between 10 Hz and 30 Hz and corresponding amplitudes of vibration are large enough to avoid the collapse of particles in the cold zone. Finally, the density profiles of experiments show that the "cold" zone is well identified and that defining the size of the "hot" zone by a different criteria -as for example 90% of the plateau value- has negligible effects on the temperature results, at least to a reasonable extent.

The second result is related to the ratio  $T_{tr}/T_{rot}$  which clearly increases with  $A\omega$  and which also depends strongly on the volume fraction of the medium. The translational temperature is about one order of magnitude larger than the rotational temperature. Again, the fact that most of the collision are quite head-on ones in this geometry, as reflected by the high value of  $T_y/T_x$  may explain why the transfer from translational to rotational energy is rather weak, especially at the lowest area fraction.

As a first step to describe the experimental behavior on granular temperatures, we can use existing theoretical models using a mean-field theory [13]. In this description, the rate of change of the temperature of a granular medium is determined through two coupled equations

$$\begin{cases} \frac{dT_{tr}}{dt} = J_{dr} + G \left[ -A T_{tr}^{3/2} + B T_{tr}^{1/2} T_{rot} \right] \\ \frac{dT_{rot}}{dt} = 2G \left[ B' T_{tr}^{3/2} - C T_{tr}^{1/2} T_{rot} \right] \end{cases}$$

Where  $T_{tr}$  and  $T_{rot}$  represent respectively the translational and rotational temperatures and  $J_{dr}$  is related to the collision rate between particles;  $G$  being the pair correlation function at contact. In two dimensions,  $G = 2\phi$ . The constants  $A$  and  $B$  depend only on the inelastic properties of the particles (more details are given in [15]).  $J_{dr}$  is the energy input into the medium and, in this analysis, the energy is supposed to be injected homogeneously into the medium. Note that these constants are positive so that the minus signs express the dissipative behavior of the medium. We consider the driving energy to act mainly on the translational part of the temperature due to the dominance of the collisions with normal incidence. In other situations where the behavior of the granular is mainly governed by rotation  $J_{dr}$  is included in the second equation of (2) [28, 29].

Several inelastic modelizations were proposed by Herbst et al. [15] going from a simple consideration of a constant tangential restitution coefficient up to more complex ones where the tangential restitution depending on  $\gamma_{12}$  (the contact angle obtained neglecting the rotational velocities) or on the real contact angle  $\gamma$ . From the second equation of (2), the energy ratio  $T_{tr}/T_{rot}$  can be obtained considering the medium in steady state  $dT_{rot}/dt=0$ , allowing to get the relation  $T_{tr}/T_{rot}=C/B'$ . In this equilibrium regime,  $dT_{tr}/dt=0$  and replacing  $T_{rot}$  in the first equation of (1) also gives  $T_{tr}=\left[CJ_{dr}/G(AC-BB')\right]^{2/3}$ . Depending on the model used, the expressions of the constant  $C$  and  $B'$  can be calculated but are only related to the inelastic properties of particles and to their inertia but neither to the area fraction nor to the driving energy flux  $J_{dr}$ . Introducing the values of the normal and tangential restitution and friction coefficient from our experiments, and solving numerically the models gives ratio of  $T_{tr}/T_{rot}$  at maximum of 5 but more important, values which are independent of the cell's velocity. Actually, these models do not deal with an anisotropic temperature because their predictions are usually compared simulations where the energy is injected in an isotropic way. This is likely the main reason for the non-ability of these models to represent correctly our experimental results.

Now, we will focus on the equilibrium temperature of the medium. When submitted to the external vibration, the medium can be modeled as a dissipative medium to which a given amount of energy is injected through the external vibration per unit time. The equilibrium temperature is obtained by solving the equilibrium equation  $J_{dr}+Q_d=0$ , where  $J_{dr}$  is the energy flux injected in the medium by the collisions of particles with the walls of the cell and  $Q_d$ , the energy flux dissipated during the binary collisions between particles.  $J_{dr}$  takes place in the regions close to the top and bottom walls, while  $Q_d$  is determined in the bulk of the medium. The experimental results obtained with our cell's geometry clearly show that the main part of the energy of the particles is distributed along the direction of the external vibration ( $y$ -direction). Based on experimental observations, we define the regions of energy injection by two layers of thickness  $h_H$  close to the top and bottom moving walls and having the same width  $L_x$ . In these two regions, the density of particles is smaller than the average density of the medium; we call  $N_H$  the average number of particles present at any time in this region. Thus, the bulk of the medium (i.e. the "cold" zone) reduces to dimensions  $h_c=L_y-2h_H$  where only particles are present at any time; the surface of this zone is then  $S_c=h_cL_x$ . In the "cold" zone, the dissipated energy depends on the collision frequency which in turns depends on the temperature of the medium. If we neglect the loss of energy coming from tangential restitution coefficient, the energy dissipated per collision is given by:

$$\Delta E_{pp} = m \frac{(r^2 - 1)}{4} \langle [(\vec{v}_1 - \vec{v}_2) \cdot \vec{n}]^2 \rangle = \frac{(r^2 - 1)}{2} T.$$

The frequency collision which is the inverse of the Enskog time is given in 2D by :

$$f_E = \sqrt{2\pi} \frac{N_C}{S_C} \sigma g_2(\varphi) \langle v \rangle = \frac{2}{N_C} f_E^N,$$

where  $N_C/S_C$  represents the number density in the “cold” region and  $f_E^N$  is the number of collisions between  $N$  particles per unit time. Finally the dissipated energy flux will be expressed as (see also appendix in (O.Herbst,2015):

$$Q_d = f_E^N \Delta E_{pp} = \frac{N_C^2}{h_C L_x} \frac{1-r^2}{2} \sigma g_2(\varphi) \sqrt{\frac{\pi}{m}} T^{3/2}.$$

Since the temperature is anisotropic, we have to replace in (4)  $T$  by  $(T_x + T_y)/2$  or  $(1 + 1/R_T)T_y/2$ , where  $R_T = T_y/T_x$  so that instead of (4) we get

$$Q_d = \frac{N_C^2}{h_C L_x} \frac{1-r^2}{4} \sigma g_2(\varphi) \sqrt{\frac{\pi}{2m}} T_y^{3/2} \left(1 + \frac{1}{R_T}\right)^{3/2}. \quad (5)$$

Now, in order to obtain an expression for the injected energy into the medium, one has to consider the energy flux generated during the collisions between the particles and the top and bottom walls of the cell. During one collision, the change in kinetic energy of one particle is: with and , respectively, are the velocities of the particle after and before collision with the cell’s wall. The cell is assumed to move with a velocity . The relative velocity equation gives where is the normal restitution coefficient between the particle and the wall. The change in kinetic energy of one particle may then be rewritten as and the energy flux ,  $h_{dr}$  associated with particles going towards the wall, can be expressed

as  $j_{dr} = \dot{c} \frac{N_H}{2h_H} v_y \Delta E(v_y, V_{dr})$  ; where we have assumed that  $N_H/2$

$N_H/2$  particles are going towards the wall. The net energy flux for a given wall velocity is then obtained by averaging the flux of the incoming particles with the velocity distribution function,

$f(v_y)$  associated with the “cold” region and integrating on the velocities directed towards the wall:

$$J_{dr}(V_{dr}) = \dot{\epsilon} \int_0^{\infty} j_{dr} f(v_y) dv_y$$

where the average value of the velocity is the one retrieved from experiments. The matching is in very good agreement and we will consider this type of behavior in the following.

The integral (5) over the velocities gives the following result

$$J_{dr}(V_{dr}) = \dot{\epsilon} \frac{m}{4} \frac{N_H}{h_H} \left[ (1+\alpha)^2 V_{dr}^2 I_1 - 2(1+\alpha) V_{dr} I_2 - (1-\alpha^2) I_3 \right]$$

$I_1$ ,  $I_2$ ,  $I_1$ ,  $I_2$  and  $I_3$ ,  $I_3$  are the integrals  $\int_0^{\infty} v_y^i f(v_y) dv_y$  ( $i=1..3$ ) which are respectively given by:

$$I_1 = \sqrt{\frac{T_y}{2\pi m}} \quad I_2 = \frac{T_y}{2m} \quad I_3 = \left(\frac{T_y}{m}\right)^{\frac{3}{2}} \sqrt{\frac{2}{\pi}}$$

In this derivation all the particles are supposed to go from the bulk towards the wall, so we have neglected the double collisions (with the particle going away from the wall and hit a second time by the wall) that we did not observe in our video records. It remains to average on the wall velocity. Then the linear term in  $V_{dr}$   $V_{dr}$  cancels and the term in  $V_{dr}^2$   $V_{dr}^2$  averages to  $(A\omega)^2/2$   $(A\omega)^2/2$  which gives the following flux for the injected energy (after multiplication by 2 for the two walls):

$$J_{dr} = m \frac{N_H}{2h_H} \dot{\epsilon} (1+\alpha)^2 (V_{dr})^2 \sqrt{\frac{T_y}{2\pi m}}$$

If  $\alpha=1$  (perfectly elastic walls), we recover the expression given by Soto [26] for a sinusoidal vibration taking for their function the constant value which is actually a very good approximation in the range of our experimental values of  $\delta$ . Note here that if g-jitter do not influence the velocities of the free floating particles, it there can nevertheless give an additional contribution to the wall velocity and so to the energy injected into the medium. This can be estimated as  $\langle \delta V^2 = 0.005 \text{ m}^2/\text{s}^2 \rangle$

[[[31]]. Since it does not exceed 15% of  $T_y$  in the worst case, it was neglected. The equilibrium between injection (Eq. (8)) and dissipation (Eq. (4)) gives:

The temperature is proportional to the square of the amplitude of the driving velocity. Since we know, for each experiment, the respective density of the “cold” and “hot” domains we can compare the theoretical predictions of Eq. (9) with the experimental values of  $T_y$  calculated in the “cold” domain. In order to take into account the dissipation due to the tangential restitution coefficient  $e_t$ , we use instead of  $e$  in Eq. (9) an effective restitution coefficient  $e_{eff}$  proposed by S. McNamara and S. Luding [32]:  $e_{eff} = \frac{1+e_t}{2}$ . Using  $e_{eff}$  for a disk and  $e_{eff} = e$ ; we obtain  $T_y$  instead of  $T$ . The comparison between the theoretical temperatures  $T_y$  obtained from Eq (9) with the experimental ones calculated in the "cold" region is presented in the figure 16.

We observe a quite good agreement for the two volume fractions we have used. In order to have a useful prediction of the relation between the temperature and the driving velocity, the main point would be to be able to predict the density  $N_H/h_H$   $N_H/H_H$  close to the wall instead of taking this value from the experimental profile as we have done in this work.

The anisotropy of the temperatures produced by a vibrating wall is scarcely studied in the literature. One can find a recent experimental study in a 3D-cylindrical configuration [33] where the anisotropy  $R_T = T_y/T_x$   $R_T = T_y/T_x$  is reported versus the volume fraction of particles and is shown to increase strongly for volume fraction below 10% but remains smaller than our values. A theoretical analysis is presented in [34] based on two different Maxwellian distributions for the directions parallel and perpendicular to the vibration and a density along the vibration axis,  $y, z$  proportional to

$$\exp\left(\frac{-mgy}{T}\right).$$

A balance between energy fluxes along and perpendicular to the direction of vibration gives the ratio  $R_T$  and predicts that, for perfectly reflective side walls, this ratio would only depend on the restitution coefficient. This is clearly not the case in our experiments (cf. table 1) where the ratio  $R_T$  is much larger at the lower density. It is not possible to directly transpose this theory to our experiments since our density profile is very different from a gravity driven one, but it may be possible to predict  $R_T$  along the same lines if we suppose a constant density in the “cold” zone.

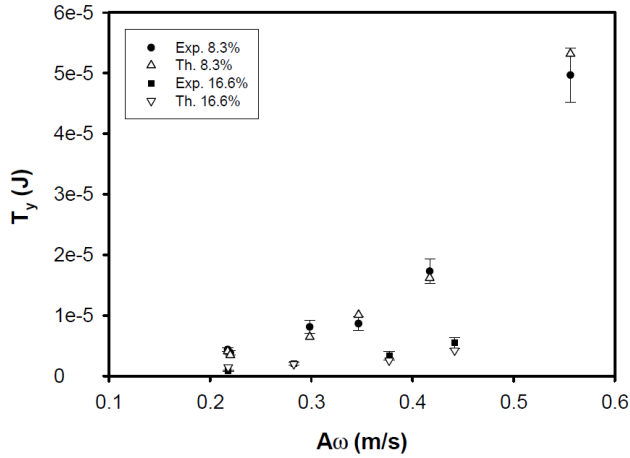


Figure 16. Comparison of the equilibrium temperature computed from eq. (9) as a function of the driving velocity of the cell ( $V_{dr}$ ).

#### 4. Conclusion

We have reported experimental investigations on the dynamics of a model granular medium. Experiments have been performed in a low-gravity environment. The cell containing the medium is subjected to external vibration which drives the collective motion of the particles. As the dynamical behavior of the medium is driven by the kinematics of the particles high-speed video recording coupled to an individual particle tracking technique allows to obtain the trajectory of each particles. From these raw data, the inelastic parameters of the particles which are at the origin of the dynamics of the whole medium can be retrieved as well as a direct measurement of the energy (or temperatures). We have found that depending on the type of particles used, the normal restitution coefficient can be dependent on the relative impact velocity between two particles but not always. One way to characterize the inelastic nature of the collisions is to look to the energy decay once the medium is freely evolving. We have obtained smaller experimental relaxation times of this energy than the ones predicted by theories at least if we do not take into account the velocity dependent of this restitution coefficient. It is also interesting to note that the effect played by the rotation of the particles can significantly affect the whole behavior of the medium. In particular we have reported the translational temperatures along and perpendicular to the direction of vibration as well as the rotational temperatures. When compared to existing theories, it appears that there are significant differences which also depends on the driving velocity and on the concentration of the medium. Two major points on the comparison can be raised: first the density is not homogeneous in experiment and second the translational velocities are much higher in the direction of vibration than perpendicular to it (versus a homogeneous input of energy as considered in theories). We have found that a balance of

the energy fluxes along the direction of vibration can represent fairly well the evolution of the temperature  $T_y$  with the driving velocity and with the volume fraction. In this balance it is necessary to take into account the contribution of the tangential velocities to the dissipation. At least the distinction between the dissipation due to the collisions between the particles which is proportional to the average temperature  $T = (T_x + T_y)/2$  and the driving flux, which depends only on  $T_y$ , was introduced, but on the basis of the experimental ratio  $T_y/T_x$ . This ratio increases when the volume fraction decreases and it also depends on the driving velocity. A theoretical determination of  $T_y/T_x$  which could reproduce these behaviors should involve the non-elastic collisions with the lateral walls, but is left for a future developments.

## 5. Acknowledgments

The authors would like to thank NOVESPACE and the CNES for giving them the possibility to board the A300-zero G in order to perform the experimental study.



## 6. References

- [1] Gondret P., Lance M. and Petit L.. Phys. Fluids. 2002;14:268.
- [2] Kantak Advait Ashok. Wet particles collisions [thesis]. University of Colorado at Boulder:2005. DOI: AAT 3190381
- [3] Sorace C. M., Louge M. Y., Crozier M. D. and Law V. H. C.. Mech. Res. Commun.. 2009;36:364.
- [4] Miller S. and Luding S.. Phys. Rev. E. 2004;69:031305.
- [5] M. Hou, R. Liu, G. Zhai, Z. Sun, K. Lu, Y. Garrabos, P. Evesque. Micrograv. Sci. Technol.. 2008;20:73.
- [6] S. Tatsumi, Y. Murayama, M. Sano. AIP Conf. Proc.. 2008;1027:923.
- [7] C. Maaß, N. Isert, G. Maret, C.M. Aegerter. Phys. Rev. Lett.. 2008;100:248001.
- [8] Y. Chen, M. Hou, P. Evesque, Y. Jiang, M. Liu. Powders & Grains. 2013;1542:791.
- [9] L. Labous, A.D. Rosato, R.N. Dave. Phys. Rev. E. 1997;56:5717.
- [10] Y. Grasselli, G. Bossis, G. Goutallier. Eur. Phys. Lett.. 2009;86:60007.
- [11] S. Das, S. Puri. Europhys. Lett.. 2003;61:749.
- [12] P. Evesque. Powders & Grains. 2001;12:60.
- [13] R. Soto. Phys. Rev. E. 2004;69:061305.
- [14] N. Rivas, S. Luding, A.R. Thornton. New J. Phys.. 2013;15:113043.
- [15] T. Jenkins, C. Zhang. Phys. Fluids. 2002;14:1228.
- [16] O. Herbst, R. Cafiero, A. Zippelius, H.J. Herrmann, S. Luding. Phys. Fluids. 2005;17:107102.
- [17] E. Falcon, J.-C. Bacri, C. Laroche. Powders & Grains. 2013;1542:815.
- [18] T.P.C. van Noije, M.H. Ernst. Granular Matter. 1998;1:57.
- [19] S. McNamara, S. Luding. Phys. Rev. E. 1998;58:813.
- [20] C.R.K. Windows-Yule, D.J. Parker. Phys. Rev. E. 2013;87:022211.
- [21] D. van der Meer, P. Reimann. Europhys. Lett.. 2006;74:384.

document.nsertBibliographyUnit